Towards quantitative magnetic information from transition metal Kedge XMCD of Prussian blue analogs

Adama N'Diaye, Amélie Bordage, Lucie Nataf, François Baudelet, Eric Rivière, Anne Bleuzen

Towards quantitative magnetic information from transition metal K-edge XMCD of Prussian blue analogs

Adama N'Diaye,[†] Amélie Bordage,[†] Lucie Nataf,[‡] François Baudelet,[‡] Eric Rivière[†] and Anne Bleuzen[†]*

[†]Institut de Chimie Moléculaire et des Matériaux d'Orsay, CNRS, Université Paris-Saclay, 91405 Orsay, France

[‡]Synchrotron SOLEIL, L'Orme des Merisiers, St Aubin, BP 48, F-91192 Gif sur Yvette, France

ABSTRACT: Two series of Prussian blue analogs (PBA) were used as model compounds in order to disentangle the information contained in X-ray Magnetic Circular Dichroism (XMCD) at the K-edges of transition metals. The number of 3d electrons on one site of the bimetallic cyanide polymer has been varied by associating to the $[Fe(CN)_6]^{3-}$ or the $[Cr(CN)_6]^{3-}$ precursors various divalent metal ions A^{2+} (Mn^{2+}, Fe^{2+}, Co^{2+}, Ni^{2+} and Cu^{2+}). The compounds were studied by X-ray diffraction and SQUID magnetometry, as well as by X-ray absorption spectroscopy and XMCD at the K-edges of the A^{2+} transition metal ion. The study shows that the 1s → 4p contribution to the A K-edge XMCD signal can be related to the electronic structure and the magnetic behavior of the probed A^{2+} ion: the shape of the signal to the filling of the 3d orbitals, the sign of the signal to the direction of the magnetic moment with respect to the applied magnetic field, the intensity of the signal to the total spin number S_A and the area under curve to the Curie constant C_A. The whole study hence demonstrates that PBAs are particularly well adapted for understanding the information contained in the transition metals K-edge XMCD signals. It also offers new perspectives towards the full disentangling of the information contained in these signals and access to new insights into materials magnetic properties.

1. INTRODUCTION

Advances in magnetic measurements are key to gain insight into magnetism and to enable novel technological applications in various fields. Therefore, techniques able to probe the magnetic properties of matter at a microscopic level such as X-ray Magnetic Circular Dichroism (XMCD) have attracted a growing interest. XMCD, having the great advantage of being element and orbital selective, has become of major importance for various scientific communities ranging from physicists to chemists or biochemists.[1-3] Nevertheless, the knowledge of the information contained in XMCD signal and therefore their interpretation strongly depends on the probed orbitals. Thus, in the case of first row transition metals, essential in the field of magnetic materials and magnetometry, it is striking that XMCD at the $L_{2,3}$ edges has become a well-established technique whereas the interpretation of XMCD at the K-edges remains at a standstill.

At the $L_{2,3}$ edges of first row transition metals probing the 3d levels, quantitative information about the spin and orbital momenta can be extracted from the XMCD signals thanks to the sum rules[4-6] and these signals are fairly reproduced by crystal field multiplet calculations.[7] Such measurements are now well established in magnetic materials science. The main drawback is inherent to the soft X-ray energy range and the detection mode. Recording XMCD signals in this energy range requires indeed ultra-high-vacuum conditions, which is incompatible with fragile samples containing solvent molecules for instance, and which reduces the sample environment flexibility. At last, owing to the detection mode and the energy range, only the surface of the sample is probed.

In contrast, although the first spin-dependent absorption in the X-ray range was observed at the K-edge of iron,[8] the interpretation of transition metals K-edges XMCD signals remains controversial. And yet, XMCD measurements in the hard X-ray range present several advantages: the delocalized character of the probed orbitals makes them (i) very sensitive to the absorber atom environment, such as subtle local structure changes or interface effects playing an important role in magnetocrystalline and surface magnetic anisotropies, the energy and high penetration depth of the X-rays are (ii) compatible with a large range of demanding sample environments, including high-pressure cells, and (iii) the measurements are bulk sensitive and not limited to the surface. XMCD signals at the transition metal K-edge is however a widely used technique and for instance the preferred technique to probe magnetism under pressure.[9-14] Nevertheless, a full interpretation of these signals is missing, despite the many efforts devoted to apply the sum rule at the K-edges,[5, 15, 16] understand and reproduce the signals, especially by using different calculation approaches.[16—24]

In this context, we are engaged in the development of an original experimental approach based on the versatile chemistry of a family of isostructural coordination compounds, the Prussian Blue Analogs (PBAs), to disentangle the processes generating the XMCD signals at the transition metal K-edges. It has to be noted that XMCD at the $L_{2,3}$ edges of transition metal ions have already been successfully used in PBAs and derivatives to determine the orbital and spin magnetic momenta by using the sum rule,[25-28] to study pressure-induced magnetic switching and linkage isomerism,[29] to determine the orientation of magnetic moments in core-shell nanoparticles[30] or to evidence

surface effect in a photo-induced state,[31] while the main information derived from XMCD at the K-edge of transition metal ions is generally limited to the relative orientation of the magnetic moments.[32]

The formula of the genuine Prussian blue is $Fe^{III}_4[Fe^{II}(CN)_6]_3 \cdot 14H_2O$.[33] Its structure, first proposed by Keggin and Miles,[33] was reformulated by Lüdi and Güdel for Prussian blue and Prussian blue analogs (PBA),[34, 35] and recently revisited to account for arrangement of vacancies.[36] Alkali cation free PBAs build a large family of compounds exhibiting the well-known face centered cubic structure of chemical formula $A_p[B(CN)_6]_q \cdot xH_2O$, where A and B are transition metal ions of the first row. A scheme of the unit cell is shown in Figure 1. Most often, the charge of the A^{q+} ions and $[B(CN)_6]^{p-}$ entities are different, so that $[B(CN)_6]^{p-}$ vacancies ensure the neutrality of the solid. When the synthesis is realized in presence of alkali cations, the latter may be trapped in the interstitial sites of the structure. This insertion is accompanied by the insertion of supplementary $[B(CN)_6]^{p-}$ entities in order to compensate the charge. Thanks to their specific structure and the variety of transition metal ions and alkali metal ions combinations that may be achieved through coordination chemistry, this family of compounds thus offers an exceptional choice of isostructural compounds in which the chemist can, at will, vary some selected parameters and analyze their effect on the XMCD signal at both K-edges of the transition metal ions. Nevertheless, it has to be noted that, given the intrinsic structural disorder of the compounds due to the presence of zeolitic water molecules and randomly distributed vacancies as well as possible small distortion of the B-CN-A linkages, the crystallographic position of all atoms, excepted that of the transition metal ions, is generally not exactly known.

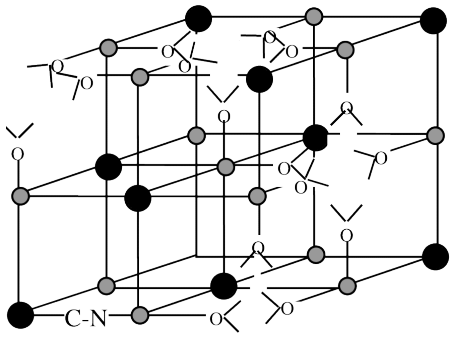

Figure 1. Scheme of the unit cell of a $A_4[B(CN)_6]_{2.7} \cdot xH_2O$ alkali cation free Prussian blue analog. Black circles stand for the B^{3+} ion (Cr^{3+} or Fe^{3+}) and the grey circles for the A^{2+} ions (Mn^{2+}, Fe^{2+}, Co^{2+}, Ni^{2+}, Cu^{2+}). The zeolitic water molecules are omitted for clarity.

In the present work, we focus on the XMCD signal at the K-edge of the A site of alkali cation free $A_4[B(CN)_6]_{2.7}$ PBAs. Two series of PBA were prepared in which the nature and amount of the $[B(CN)_6]^{p-}$ unit has been fixed, while the nature of the A^{2+} cation has been varied. The chemical compositions of both series are $A^{II}_4[Fe^{III}(CN)_6]_3 \cdot nH_2O$ (A^{2+}=Mn^{2+}, Co^{2+}, Ni^{2+}, Cu^{2+}) and $A^{II}_4[Cr^{III}(CN)_6]_3 \cdot nH_2O$ (A^{2+}=Mn^{2+}, Fe^{2+}, Co^{2+}, Ni^{2+}) ; these two series of compounds are respectively called **AFe** and **ACr** in the following. Our goal here is to analyze the effect of a change in the number of unpaired electrons and of magnetic orbitals of the A site on the XMCD signal at the A K-edge. In order to be able to precisely assign the features of the XMCD signals, the A K-edge X-ray absorption spectra of both series were also recorded. The compounds were investigated by SQUID magnetometry for the XMCD signals to be related to the macroscopic magnetic properties. The study shows that PBA are well-suited model compounds to get new insight into XMCD and, in turn, XMCD can provide original quantitative and qualitative information on molecular materials.

2. EXPERIMENTAL SECTION

Two series of four $A_4[Fe(CN)_6]_{2.7}$ and $A_4[Cr(CN)_6]_{2.7}$ PBAs were synthesized. The **AFe** and **ACr** series are respectively composed of $Mn_4[Fe(CN)_6]_{2.7}$ (called **MnFe**), $Co_4[Fe(CN)_6]_{2.7}$ (called **CoFe**), $Ni_4[Fe(CN)_6]_{2.7}$ (called **NiFe**), $Cu_4[Fe(CN)_6]_{2.7}$ (called **CuFe**) on the one hand, and $Mn_4[Cr(CN)_6]_{2.7}$ (called **MnCr**), $Fe_4[Cr(CN)_6]_{2.7}$ (called **FeCr**), $Co_4[Cr(CN)_6]_{2.7}$ (called **CoCr**), $Ni_4[Cr(CN)_6]_{2.7}$ (called **NiCr**) on the other hand. EDS analyses, powder X-ray Diffraction and magnetic measurements were performed using the devices of the ICMMO instrumentation platform.

2.1 Sample preparation. The eight PBAs were synthesized by a drop-by-drop addition of two precursors in aqueous solutions: a 400 mL aqueous solution of potassium hexacyanoferrate(III) $K_3[Fe(CN)_6]$ or potassium hexacyanochromate(III) $K_3[Cr(CN)_6]$ ($c = 2.5.10^{-3}$ $mol.L^{-1}$) was added to a 100 mL aqueous solution of nitrate salts $A(NO_3)_2$ (A = Mn, Fe, Co, Ni, Cu; $c = 50.10^{-3}$ $mol.L^{-1}$). The precipitates were washed with distilled water and centrifuged three times at 8000 rpm, and finally allowed to dry in air at room temperature.

2.2 Energy Dispersive Spectroscopy (EDS) analyses. The chemical formulas of the eight PBAs were checked by EDS analyses, using an EDS spectrometer installed on a ZEISS Sigma HD microscope. Data processing was done using the IDFix EDS analysis software. The results are given in S1 and S2 for the series **AFe** and **ACr** respectively.

2.3 Powder X-Ray Diffraction (XRD). Powder XRD data were collected with a Philips X'Pert diffractometer (Cu $K\alpha_1$ radiation) at room temperature. All diagrams were recorded over the 10-70° 2θ angle range with steps of 0.01°. An aluminum sample holder was used for all measurements. The cell parameters were extracted by a Lebail refinement procedure (using the Fullprof software), considering a Fm3m space group. The XRD patterns and corresponding cell parameters for the **AFe** and **ACr** series are given in S1 and S2 respectively.

2.4 SQUID magnetometry. Magnetic properties were investigated using a Quantum Device XL-7 SQUID magnetometer. 5.6 mg of PBA powder was placed in a capsule and 17 mg of eicosane were added to ensure that the particles would not move with the application of the magnetic field. Field Cooled-Zero Field Cooled (FC-ZFC) measurements were performed over the 2K-100K temperature range under a 30 Oe magnetic field. In order to determine the Weiss temperature (Θ), the magnetization was measured as a function of temperature up to 300K under a 5000 Oe magnetic field; the experimental curves were fitted using a Curie-Weiss law (S4 and S6). Finally, the magnetic field dependence of magnetization was recorded at 4K for a magnetic field varying between -40000 Oe (-4 T) and 40000 Oe (4 T).

2.5 Transition metal K-edge XAS. X-ray Absorption spectra in the transmission mode were recorded for both series at the A K-edge on the SAMBA beamline[37] at SOLEIL (Gif sur Yvette, France). We used a Si(220) monochromator and recorded the spectra in a continuous mode. Measurements were performed at room temperature on pellets. We carefully checked that no radiation damage occurred. Following the measurements, the spectra were energy-calibrated and conventionally normalized using the ATHENA software.[38] To more easily compare them, the A K-edge XANES spectra are plotted in the following as a function of E-E0, E0 being defined here as the energy of the absorption maximum.

2.6 Transition metal K-edge XMCD. X-ray Absorption spectra and XMCD signals were recorded at the Mn, Fe, Co, Ni and Cu K-edges in the transmission mode using the dispersive setup of the ODE[39] beamline at SOLEIL (Gif sur Yvette, France). The measurements and normalization procedure are presented and discussed in details in Ref. 40, and we recall here only the main information. We used a Si(311) polychromator in order to get a high resolution in the white line region of the spectra. Measurements were strictly performed at 4 K using a He-cooled cryostat in order to be well below the Curie temperature of the eight PBAs and to avoid any artifact in the intensity related to a change in the temperature. An external magnetic field of 1.3T, generated by an electromagnet, was applied alternatively parallel and antiparallel to the direction of the photon beam. Samples of the **AFe** series were placed in a Diamond Anvil Cell (with no pressure-transmitting medium); in the case of PBAs, it ensures an optimized homogeneity of the sample. For the **ACr** series, the diamonds were replaced by Plexiglas strip to minimize the absorption of the beam and retain a brilliant enough flux at the Cr K-edge to be able to perform the measurements. Attenuators of appropriate thickness were placed before the sample to avoid radiation damage. A metallic foil was recorded at each edge for energy calibration.[40] The circular polarization rate is identical for all the edges. The XANES spectra and XMCD signals were normalized as described in Ref. 40. Like for the X-ray absorption spectra from SAMBA, they are represented as a function of E-E0, with the same definition of E0.

3. RESULTS

3.1 Magnetic study. A magnetic study of the compounds was performed prior to the XMCD investigation in order to get insight into their macroscopic magnetic behavior and to determine some useful parameters such as the magnetic ordering temperature (T_C), the Curie constant for one unit cell of PBA (C_{PBA}) or the sign of the magnetic coupling constant (J). The magnetization curves versus the magnetic field at 4 K, temperature at which the XMCD measurements were performed, are shown in Figure 2a and 2b for the compounds of the **AFe** and **ACr** series respectively. The Field Cooled (FC) and Zero Field Cooled (ZFC) magnetization curves, as well as the temperature dependence of the inverse of magnetic molar susceptibilities, are given in S3 and S4 for the **AFe** series, and S5 and S6 for the **ACr** series. T_C was determined as the temperature of a minimum in the derivative of the FC magnetization curve ($dM_{FC}(T)/dT$; S3 and S5). The Curie (C_{PBA}) and Weiss (Θ) magnetic constants were extracted from the plots of the inverse of the molar susceptibility versus temperature by fitting a Curie-Weiss law to the curves (S4 and S6). All these magnetic data as well as the coercive field (H_C) at 4 K are gathered in Table 1.

The T_c value is above 4 K for all compounds, which are therefore all in a magnetically ordered state at 4 K. As a first approximation, for transition metal ions of the first row, magnetic moments are considered originating from the spin angular momentum. In the magnetically ordered state, the orientation of the magnetic moments with regard to an applied external magnetic field can thus be predicted from the total spin quantum number of the ions and from the sign of J. For each PBA, the magnetic moment of the ion with the largest total spin quantum number aligns in the direction of the magnetic field and the second one is parallel (J>0) or antiparallel (J<0) to the former depending on the sign of J. In such compounds where exchange interactions prevail, the sign of Θ directly gives the sign of J. The direction of the magnetic moments in an external magnetic field is schematized in Figure 3 for all compounds. Whatever the sign of J, the magnetic moment carried

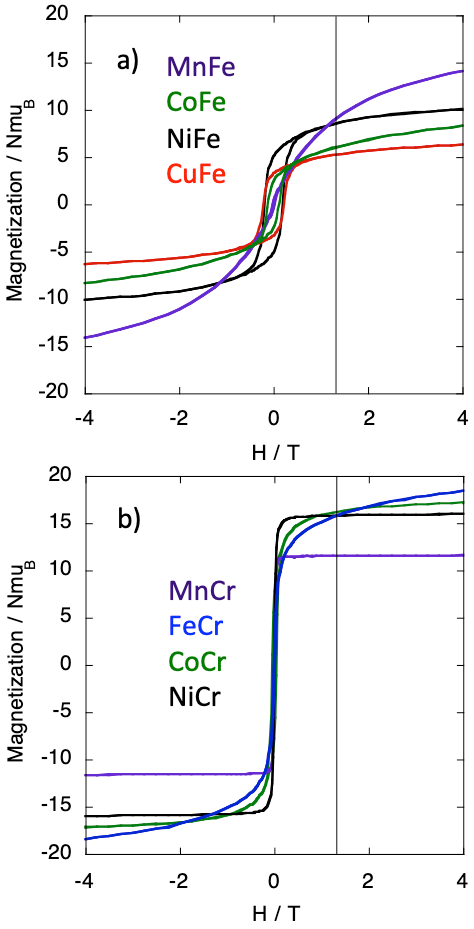

Figure 2. Magnetic field dependence of the magnetization at 4K for a) the **AFe** series and b) the **ACr** series. The vertical line indicates the magnetic field value used for XMCD measurements (1.3 T).

	T_c *K*	C_{PBA} *$cm^3.mol^{-1}$*	Θ *K*	M_{sat} calc $N\mu_B$	M (4T) $N\mu_B$	M (1.3T) $N\mu_B$	H_c *10^{-4} T*
MnFe	12	18.5	-12	17.3	14.1	9.1 (53%)	246
CoFe	14	14.2	-9	9.3	8.3	6.2 (67%)	1240
NiFe	22	6.6	32	10.7	10.1	8.5 (79%)	2000
CuFe	19	3.3	38	6.7	6.3	5.3 (79%)	2250
MnCr	64	19.1	-38	11.9	11.7	11.7 (100%)	10
FeCr	16	18.6	24	24.1	18.4	16 (66%)	175
CoCr	25	15.8	43	20.1	17.1	16.3 (81%)	550
NiCr	65	10	85.5	16.1	16	16 (100%)	67

Table 1. Curie temperature (T_C), Curie (C_{PBA}) and Weiss (Θ) constants, calculated saturation magnetization (M_{sat}), experimental magnetization at 4 T (M(4K)) and 1.3 T (M(1.3T), and coercive field (H_C) for both AFe and ACr series of compounds.

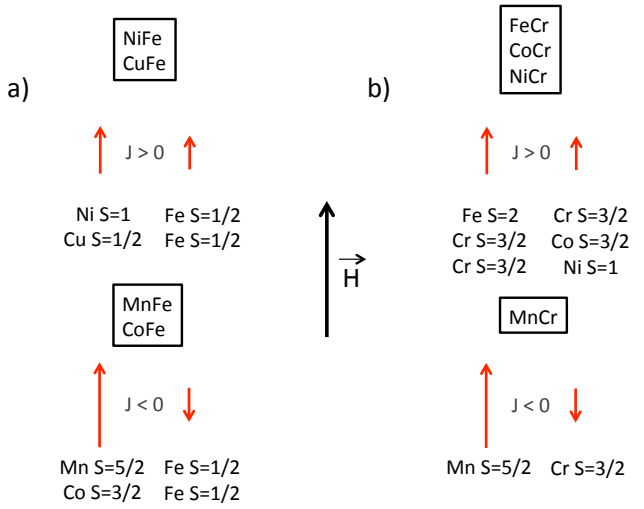

Figure 3. Anticipated orientation of the magnetic moments carried by the transition metal ions in an applied magnetic field H for the a) **AFe** series and b) **ACr** series.

by the A^{2+} ion is expected to be oriented in the direction of the applied magnetic field for all compounds. Regarding the dependence of the magnetization versus magnetic field (Figure 2), it can clearly be seen that the magnetization of most compounds does not reach saturation even at 4 T, while the magnetization of **NiCr** and **MnCr** saturates at magnetic fields as low as 0.2 T. The saturation magnetization (M_{sat}) for one unit cell can be calculated from eq 1 in $N\mu_B$ unit, where N is the Avogadro constant, μ_B the Bohr magneton and g the electron g-factor (g=2):

$$M_{sat} = g[4S_A \pm 2.7S_B] \quad (1)$$

The sign ± depends on the nature of the exchange interaction (+ for J>0 ; - for J<0). 4 and 2.7 are the numbers of A and B ions in a unit cell respectively, S_A and S_B the total spin quantum numbers of the A^{2+} and B^{3+} ions. The calculated value for M_{sat} as well as the experimental magnetization at 4 T (the highest field reached by the magnetometer) and at 1.3 T (the magnetic field used for the XMCD measurements) are gathered in Table 1. For **NiCr** and **MnCr**, M_{sat}, M(4T) and M(1.3T) are equal. The saturation is reached. For all other compounds, the saturation magnetization is not reached. M(4T) and M(1.3T) are thus lower than M_{sat} and the saturation percentage at 1.3 T ((M(1.3T)/M_{sat})*100) is also given in bracket in Table 1. It must be noticed that **MnFe** shows a specific behavior among the compounds with a magnetization at 1.3 T much lower than the saturation (only ≈ 50% of the expected value), while the magnetization of all other compounds reaches values at 1.3 T at least around 70% of the expected saturation value. For all compounds, the magnetic field dependence of the magnetization is in agreement with the nature of the exchange interaction and the sign of J deduced from the Curie-Weiss law.

3.2 A K-edge XMCD spectra. The XMCD signals at the A K-edges are shown as a function of E-E0 in Figure 4a and 4b for the **AFe** and **ACr** series respectively. The XMCD signals are all different but they can be divided into three energy

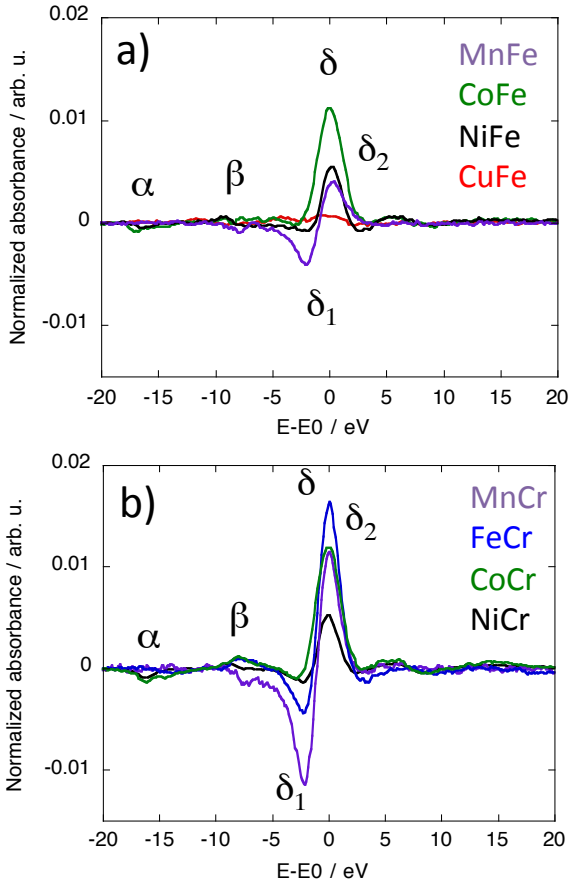

Figure 4. Normalized XMCD signal at the A K-edge recorded at 4K as a function of (E-E0) over the -30 +30 eV energy range for the compounds of a) the **AFe** series and b) the **ACr** series.

Sample	Absolute value of the normalized intensity				α/δ %
	α	δ_1	δ_2	$\delta_1+\delta_2$	
MnFe	0.0001	0.004	0.004	0.008	2.5
CoFe	0.0008	-	0.0115	0.0115	7
NiFe	0.0005	0.0007	0.005	0.006	9
CuFe	-	-	0.0006	0.0006	-
MnCr	0.00045	0.0115	0.0115	0.023	4
FeCr	0.0005	0.004	0.016	0.02	2.5
CoCr	0.0001	-	0.012	0.012	8
NiCr	0.00085	-	0.005	0.005	15

Table 2. Absolute value of the intensity of the α and δ contributions to the XMCD signals of the AFe and ACr series of compounds.

ranges. For all compounds, XMCD gains intensity i) over the -20 to -12 eV energy range (α peaks), ii) over the -12 to -5 eV energy range (β peaks) and iii) over the -5 to 4 eV energy range (δ peaks). In order to clearly assign these different contributions, the XMCD signals were compared to the XANES spectra at the A K-edges (S7), which all exhibit the profile expected for 6-fold coordinated A^{2+} ions in their high spin state and are typical of A K-edge XANES spectra of PBAs.[41] A very close local structure around the A^{2+} ions from one compound to the other is confirmed by comparable oscillations in the EXAFS part of the spectra (S8). The comparisons of the XANES spectra and XMCD signals are enlarged in Figures 5a-j.

Over the -5 to 4 eV energy range corresponding to the edge region of the XANES spectra, the main contribution to the XMCD signal (δ peaks, Figures 4a and 4b) is composed of two lobes: a low-energy negative lobe (δ_1) and a high-energy positive one (δ_2). The absolute value of the intensity of the two lobes as well as their sum is given in table 2. It is noticeable that the intensity of the δ peaks of **CuFe** (Figure 4a) is very low compared to that for all other compounds. The maximum intensity of the δ_2 peak is located at the energy of the absorption maximum of the XANES spectra for all compounds (Figure 5b, 5d, 5f, 5h and 5j). The main contribution to the XMCD signal can therefore be assigned to the electric dipole 1s → 4p transitions, 4p orbitals being spin-polarized by the 3d electrons. XMCD gains intensity from the electric dipole allowed 1s → 4p transitions for all compounds. The features of this main contribution to the XMCD signal are discussed in the following.

Over the -12 to -5 eV energy range corresponding to the rising edge region of the XANES spectra (Figure 4a and 4b), the XMCD signals of all compounds gain intensity (β peaks) at the same energy as the β peak of the XANES spectra (Figure 5a, 5c, 5e, 5g and 5i). These peaks can be assigned to 1s → π*(NC) transitions[32] but an assignment to shake-down transitions[42-44] arising from the ligand-to-metal charge transfer induced by the core-hole creation cannot be ruled out. Whatever the origin of these transitions a contribution from the electric dipole 1s → 4p transitions is expected in octahedral or pseudo-octahedral symmetry. A contribution to the XMCD signal over this energy range is therefore not surprising as XMCD gains intensity from 1s → 4p transitions.

Over the -20 to -12 eV energy range (Figures 4a and 4b), the XMCD signals of all compounds gain intensity (α peaks) at the same energy as the α pre-edge peak of the XANES spectra (Figures 5a, 5c, 5e and 5g). In a centro-symmetric environment of the absorber atom, the pre-edge peaks of the XANES spectra are assignable to the electric quadrupole 1s → 3d transitions. Nevertheless, in PBAs the A^{2+} ions are surrounded by an average of 4 –NC and 2 $–OH_2$ ligands, so that most of the A sites are not centro-symmetric. Thus 3d-4p orbitals mixing and therefore a contribution from the electric dipole 1s → 4p transitions is expected over this energy range. For **CuFe**, the intensity of the XMCD signal over the pre-edge energy range hardly overcomes the signal-to-noise ratio in our measurements conditions. **CuFe** is also the compound for which the intensity of the δ peak associated with the 1s → 4p transitions

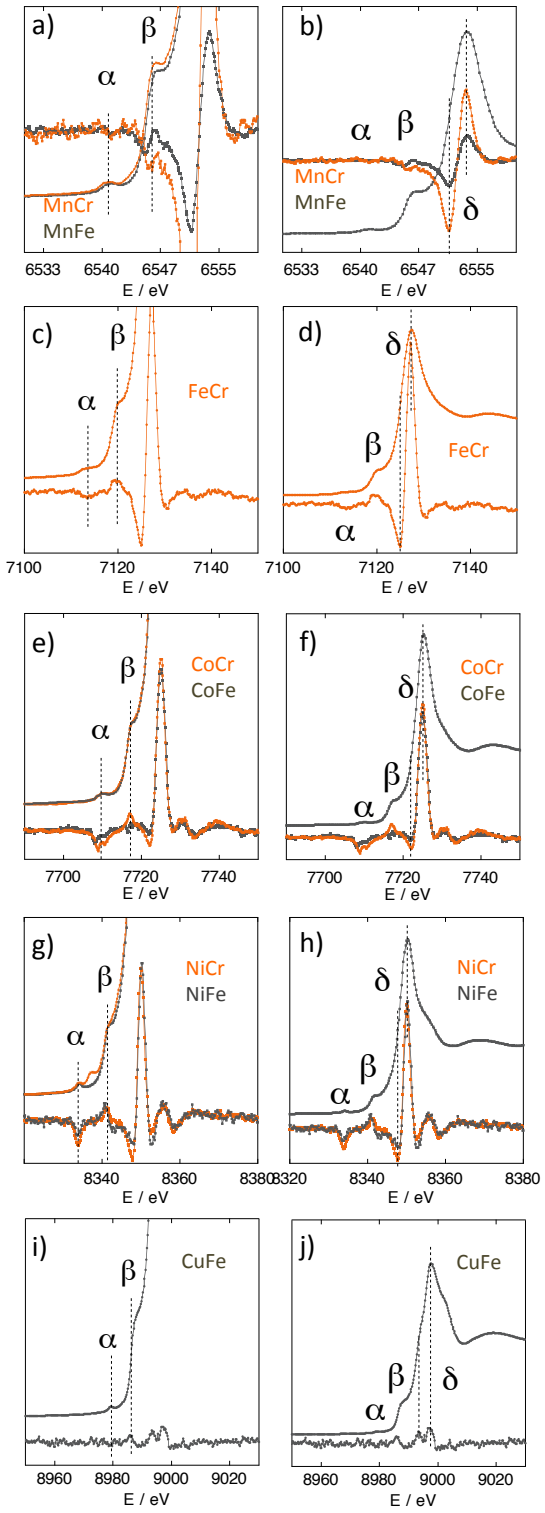

Figure 5. XMCD signal compared to the adapted enlargement of the XANES spectrum over the pre-edge/rising edge and edge regions for a, b) **MnCr** and **MnFe** at the Mn K-edge, c, d) **FeCr** at the Fe K-edge, e, f) **CoCr** and **CoFe** at the Co K-edge, g, h) **NiCr** and **NiFe** at the Ni K-edge and I, j) **CuFe** at the Cu K-edge.

is the lowest, which suggests that XMCD would mainly gain intensity from the 1s → 4p transitions over the pre-edge energy range. At last, the pre-edge region of the XMCD signals is similar for all **AFe** and **ACr** couples of compounds (**MnCr** and **MnCr**, **CoCr** and **CoFe**, **NiCr** and **NiFe**), reflecting a very close electronic structure of the 3d orbitals in these couples of compounds despite a different B^{3+} ion (Fe or Cr) on the other side of the NC bridge.

4. DISCUSSION

XMCD signals at the transition metal K-edges of PBAs have already been reported in the literature. Nevertheless, the main information that has been extracted from them so far is the direction of the magnetic moment carried by the absorber atom in the applied magnetic field. In a first step, we will use the model compounds as a tool to disentangle the information contained in the XMCD signal by trying to relate some features of the signal to magnetic data. In a second step, we will discuss the opportunities that can be expected from such measurements in terms of magnetic molecular materials study.

4.1 PBAs as model compounds for the understanding of transition metal K-edge XMCD signal.

It has to be recalled that previous studies showed that XMCD at the transition metal K-edge is a probe of the 4p orbital momentum.[4,20] The 4p orbitals are nevertheless polarized by the magnetic moment arising from the 3d electrons, the number of which has been varied at the A site in the series of compounds under study. So, by varying this electron number, we expect to highlight its influence on the XMCD signal, which reflects its influence on the 4p orbital momentum. The features of the main contribution to the XMCD signals are discussed in the following.

Sign of the signal. The sign of the XMCD peaks corresponding to the 1s → 4p transitions at the K-edge of transition metal ions in PBAs has already been related to the sign of the high-energy lobe and assigned to the direction of the magnetic moments due to the 3d unpaired electrons of the absorber atom.[32] This can be verified here too. The sign of the δ_2 high-energy lobe of the main contribution is the same at the A K-edge for all compounds. The magnetic moment born by the A^{2+} ion is oriented in the direction of the applied magnetic field for all compounds (Figure 3). As a matter of convention, the sign of the lobe δ_2 of a dichroic signal of an ion carrying a magnetic moment aligned in the same direction as the applied magnetic field has been taken as positive.

Shape of the signal. Regarding the shape of the main contribution to the XMCD signals, the compounds can be classified in two groups, depending on the relative intensity of the two lobes (low-energy negative-intensity δ_1 and high-energy positive-intensity δ_2). On the one hand, the XMCD signals of **MnCr** and **MnFe** both exhibit a derivative shape (two lobes δ_1 and δ_2 of the same absolute value of intensity). On the other hand, for all other compounds, the main contribution consists of one main high-energy positive lobe (S9). As examples, Figure 6 shows the derivative-shape of the XMCD signal of **MnFe** and the one of **CoFe** with a predominant high-energy lobe.

The belonging of the XMCD signal to one of these two groups depends on the place of the element in the periodic table of elements. Thus, the derivative-shape of the signal at the Mn K-edge of **MnCr** and **MnFe** resembles those of the signals of first-row early transition elements already reported in the literature for PBAs (Mn^{2+}, V^{2+}, V^{3+}, Cr^{3+}).[32, 45-48, 43] For the other compounds, the shape of the main peak (δ) seems to be characteristic of first-row late transition elements (Co^{2+}, Ni^{2+}, Cu^{2+} …).[46, 49-51]

Mn and Fe thus seem to be pivotal elements. The XMCD signal of Mn^{2+}(HS) in **MnCr** still belongs to the first group, while the one of Fe^{2+}(HS) in **FeCr** belongs to the second one (Figure 4). The main differences between these two ions are i) the atomic number Z and ii) the arrangement of the electrons in the t_{2g} and e_g orbitals. In Mn^{2+}(HS) as in early transition metal ions, the t_{2g} and e_g orbitals are half-filled or less than half-filled, whereas in Fe^{2+}(HS) as in the late transition metal ions, some of

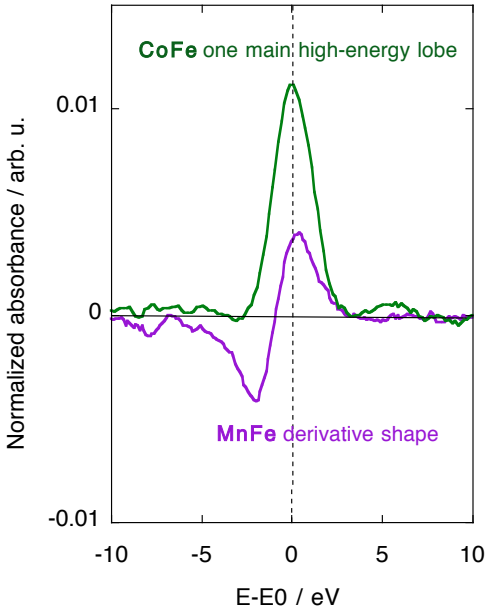

Figure 6. XMCD signals of **MnFe** at the Mn K-edge (derivative shape) and **CoFe** at the Co K-edge (one main lobe).

these orbitals are more than half-filled. The Fe^{3+} ion is therefore a good candidate to identify between the two parameters, Z and the arrangement of the electrons in the t_{2g} and e_g orbitals, the determinant one. Z is that of the Fe atom. In the Fe^{3+}(HS) ion, the arrangement of the electrons in the t_{2g} and e_g orbitals is the same as in the Mn^{2+}(HS) ion; in the Fe^{3+}(LS) ion, the t_{2g} orbitals is more than half filled, whereas the e_g orbitals are empty. The shape of the Fe K-edge XMCD signal of the Fe^{3+}(LS) ions in the $Fe(CN)_6$ entities in PBAs is similar whatever the nature of the associated A^{2+} ion (S10), and its shape with two lobes of different intensities for the main peak (δ) places the XMCD signal of the Fe^{3+}(LS) ion in the second group. The Fe^{3+}(HS) ion is found in the Prussian (or Berlin) green FeFe PBA of chemical formula $Fe^{III}_4[Fe^{III}(CN)_6]_4 \bullet nH_2O$[52] synthesized following the procedure

described in ref. 52. This compound contains both Fe^{3+}(HS) ions and Fe^{3+}(LS) ions. To isolate the Fe^{3+}(HS) XMCD signal, a variable amount of the XMCD signal of the Fe^{3+}(LS) ions was subtracted to the normalized XMCD signal of the Berlin green by linear combination. A derivative shape of the main contribution with an intensity of the order of magnitude expected for an S=5/2 ion appears (S11), suggesting that the XMCD signal of the Fe^{3+}(HS) ion belongs to the first group, and that the key parameter for the shape of the signal is the filling of the t_{2g} and e_g orbitals. A derivative shape of the signal is hence associated with a same spin quantum number for all electrons in the 3d orbitals (Fe^{3+}(HS)). In contrast, a signal with one predominant lobe for the main contribution is observed as soon as two electrons are paired in the 3d orbitals, whether it is due to a more than half-filled 3d shell in weak ligand field (Fe^{2+}(HS)) or an electron pairing energy less than the crystal field parameter in strong ligand field (Fe^{3+}(LS)).

Intensity of the signal. At first glance, it can be seen on Figure 4a and 4b that, except for **MnCr** and **MnFe**, the intensity of peak δ_2 steadily increases as the total spin quantum number of the A^{2+} ion in its ground state (S_A) increases along both series of compounds. The intensity of peak δ_2 (called I^A in the following) is plotted against S_A in Figure 7.

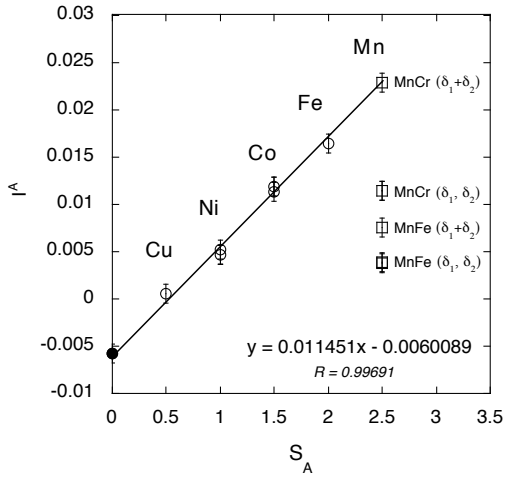

Figure 7. Intensity (I^A) of the 1s → 4p XMCD signal (peak δ_2) at the A K-edge versus the total spin quantum number S_A for **FeCr**, **CoCr**, **CoFe**, **NiCr**, **NiFe** and **CuFe** (open circles). The norm of the intensity of the positive (δ_2) and negative (δ_1) lobes of the XMCD signal at the Mn K-edge of **MnCr** and **MnFe**, as well as their sum, are indicated as open squares. The added point ((0, $-P^A_{h\nu}/2$), see text) is indicated as a black circle.

For **MnCr** and **MnFe**, the absolute value of the intensity of each lobe (δ_1 and δ_2, Figure 4a and 4b) as well as the sum of both are indicated as white squares in Figure 7. This I^A=f(S_A) plot shows, within the error bar (± 0.001), a linear dependence between the intensity of peak δ_2 and the total spin quantum number of the A^{2+} ion for **FeCr**, **CoCr**, **CoFe**, **NiCr**, **NiFe** and **CuFe**. As expected from the plots of the XMCD signals on Figure 4a and 4b, the intensity of peak δ_2 of **MnCr** and **MnFe** does not follow the same trend. Nevertheless, it is noticeable that the point corresponding to the sum of the absolute value of the intensity of peaks δ_2 and δ_1 of **MnCr** (also called I^A in the following) fits into the linear variation, which is not the case for **MnFe**. This particular case of **MnFe** is discussed later.

So, for all compounds except **MnFe**, Figure 7 shows that I^A is proportional to the total spin quantum number of the absorber atom and can be expressed by eq 2 as:

$$I^A = S_A * P^A_{h\nu} + Cst \qquad (2)$$

where S_A is the total spin quantum number of the A^{2+} ion in its ground state, $P^A_{h\nu}$ is a coefficient of proportionality and *Cst* is a constant. This indicates i) that the 4p orbitals of the A^{2+} ion are spin polarized in the same way by the unpaired electrons in the 3d shell through intra-atomic interaction for all compounds, and ii) that the XMCD signal at the A K-edge does not depend on the nature of the magnetic neighbour of the A^{2+} ion (Fe^{3+}(S=1/2) in the **AFe** series or Cr^{3+}(S=3/2) in the **ACr** series). XMCD at the A K-edge in the **AFe** and **ACr** series only depends on the magnetic properties of the A^{2+} ion or of the A^{2+} sub-lattice. It is remarkable that XMCD at the A K-edge is not affected by the magnetic moment carried by the $B(CN)_6$ entities. From eq 2, it also appears that I^A is the sum of two terms: a first one directly depending on the total spin of the A^{2+} ion in its ground state, and a second one identical for all compounds. It is also remarkable that the value of *Cst* is very close (within the error bar) to $-P^A_{h\nu}/2$ (-0.006 ± 0.001), so that I^A can be re-expressed as follows:

$$I^A = (S_A - 1/2) * P^A_{h\nu} \qquad (3)$$

The point $(0, -P^A_{h\nu}/2)$ is added on Figure 7 as a black circle; it nicely takes place into the linear trend. With the same constant term $-P^A_{h\nu}/2$ in the expression of I^A for the seven compounds, the number ½ in eq 3 can be assigned either to the spin angular momentum (s) or to the total angular momentum (j) of the photoelectron. Eq. 3 also suggests that $P^A_{h\nu}$ is the same for all compounds and for all probed A K-edges. Given the constant circular polarization rate on the ODE beamline in the energy range of the 3d transition metal K-edges, which was discussed in Ref. 40, we also suggest that the $P^A_{h\nu}$ parameter contains this circular polarization rate and external parameters such as the temperature and the magnetic field.

It is striking that, despite the fact that the saturation magnetization is not reached at 1.3 T for most of the samples with different gaps between their magnetization at 1.3 T and the saturation magnetization (Table 1), I^A, the intensity of peak δ_2 (or the sum of the absolute value of the intensity of peaks δ_1 and δ_2 for **MnCr**), linearly depends on S_A, the total spin quantum number of the A^{2+} ion. This shows that, if XMCD at the transition metal K-edge and SQUID magnetometry measure some magnetic characteristics of the sample, they do not give access to the same magnetic data. In a SQUID magnetometer, the projection of the magnetic moment onto the applied magnetic field direction is measured and therefore, the measured component depends on the angle between the magnetic moment and the applied magnetic field as long as the saturation magnetization is not reached. This is clearly not the case for the intensity of the transition metal K-edge XMCD signal corresponding to the 1s → 4p transitions (at least as soon as

the magnetization of the sample is above a certain threshold such as the closure of the hysteresis loop[40] or the coercive field[53]).

Area under the signal. We tried to plot as a function of S_A the area under peak δ_2 (called $A(\delta_2)$), under peak δ_1 (called $A(\delta_1)$), their sum $A(\delta_1)+A(\delta_2)$ and their difference, without a clear trend appearing. However, in the case of their sum $A(\delta_1)+A(\delta_2)$ (called A^A in the following), the behavior of the compounds **CoCr**, **CoFe** and **FeCr** seems to differ from the others one. Since these compounds are those for which the A^{2+} ion exhibits first-order orbital momentum (T ground state), we also tried to plot A^A as a function of the Curie constant of the A^{2+} ion (called C_A in the following). C_A was determined from C_{PBA} (Table 1) and its expression for one PBA unit cell given by eq 4:

$$C_{PBA} = 4C_A + 2.7C_B \quad (4)$$

where C_B (B=Fe, Cr) is the Curie constant of the Cr^{3+} or Fe^{3+} ion. The Cr^{3+} ion in octahedral geometry exhibits no first-order orbital momentum, so that C_{Cr} can be calculated from the spin contribution (C_{Cr} =1.875). In contrast, the Fe^{3+}(LS) ion exhibits first-order orbital momentum, and C_{Fe} was already experimentally deduced from the Curie constant of the ZnFe PBA containing diamagnetic Zn^{2+} ions (C_{Fe}=0.95).[54] The plot of A^A as a function of C_A is displayed in Figure 8 for **MnCr**, **FeCr**, **CoCr**, **CoFe**, **NiCr**, **NiFe** and **CuFe**.

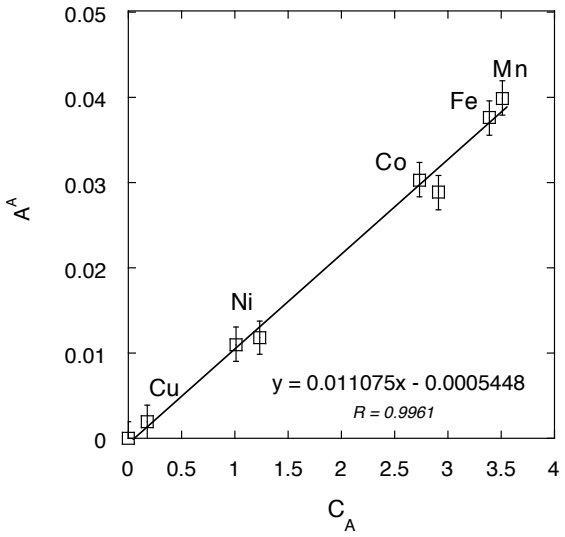

Figure 8. Area under peak (A^A) as a function of the Curie constant (C_A) for **MnCr**, **FeCr**, **CoCr**, **CoFe**, **NiCr**, **NiFe** and **CuFe**.

The plot shows that, within the error bar (±0.002), A^A linearly depends on C_A, the Curie constant of the A^{2+} ion. It is noticeable that i) the straight correlation line passes through the origin, and ii) the value of the slope is similar, within the error bar, to the one of the I^A versus S_A linear function (Figure 7). A^A can thus be expressed as follows:

$$A^A = C_A * P_{h\nu}^A \quad (5)$$

where $P_{h\nu}^A$ is the same constant as in eq 2 and 3.

This shows that the area under curve (A^A) does not depend on the fact that the saturation magnetization is not reached for several compounds, as it is also the case for the intensity (I^A) (see above). Contrary to SQUID magnetometry, which gives access to the projection of the magnetic moment onto the applied magnetic field direction and therefore strongly depends on the angle between the directions of the magnetic moment and of the magnetic field, the main features of the 1s → 4p contribution to the XMCD signal do not depend on this parameter, but probably rather on the angle between the magnetic moment and the crystallographic axes, which also are the axes of the probed 4p orbitals.

Eq 3 and 5 suggest the following relation between I^A and A^A:

$$I^A = ((S_A - 1/2)/C_A) * A^A \quad (6)$$

The plot of $((S_A\text{-}1/2)/C_A)*A^A$ as a function of I^A (Figure 9) fully confirms this relation and the previously established linear correlations on which it is based.

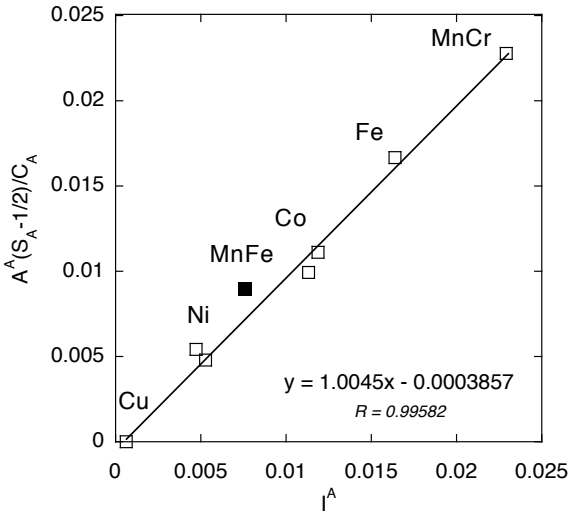

Figure 9. : $A^A(S_A\text{-}1/2)/C_A$ as a function of I_A for **MnCr**, **FeCr**, **CoCr**, **CoFe**, **NiCr**, **NiFe**, **CuFe** (white square) and **MnFe** (black square).

The features of the Mn K-edge XMCD signal of **MnFe** do not follow the same trends as those of the other PBAs of the **AFe** and **ACr** series. For all compounds except **MnFe**, eq 6 is obtained from eq 3 and 5, which apply for the samples **MnCr**, **FeCr**, **CoCr**, **CoFe**, **NiCr**, **NiFe** and **CuFe**. For **MnFe**, the intensity could not be directly related to S_A, neither the area under peak to C_A. Nevertheless, the use of eq 6 to determine the C_A value for the Mn^{2+}(HS) ion in **MnFe** (S_A=5/2) from I^A (0.0076) and A^A (0.0157) gives a value of C_A=4.1, which is very close to the value obtained from the magnetic measurement (C_A=4.0) and the calculated value for a spin only contribution (4.375). The point corresponding to the $A^A(S_A\text{-}1/2)/C_A$ and I^A values for **MnFe** has been added as a black square in Figure 9. It falls very close to the straight line formed by the points corresponding to the other compounds. This shows that eq 6 also applies to **MnFe** despite its peculiar behavior. This confirms that the Mn ion in **MnFe** carries the magnetic moment expected for the Mn^{2+} high spin ion with a total spin

quantum number S=5/2. This is in agreement with all characterizations of **MnFe** discussed above, which leave no doubt about the structure and the chemical composition of the compound or about the oxidation and spin states of the Mn^{2+} ion. Hence, I^A and A^A for **MnFe** differ from I^A and A^A for the other compounds of the **AFe** and **ACr** series by the value of $P_{h\nu}^A$. This $P_{h\nu}^{Mn}(\boldsymbol{MnFe})$ value for **MnFe** can be deduced from eq 7:

$$P_{h\nu}^{Mn}(\boldsymbol{MnFe}) = (I^{Mn}(\boldsymbol{MnFe})/I^{Mn}(\boldsymbol{MnCr}))P_{h\nu}^{A} = (1/3)\,P_{h\nu}^{A}(7)$$

Without no doubt either about the magnetic moment carried by the Mn ion or about the measurement conditions which were exactly the same, the different value of the $P_{h\nu}^A$ factor for the Mn^{2+} ion in **MnFe** and in **MnCr** can be assigned to a different orientation of the magnetic moment with regard to that of the crystallographic axes. This raises new questions about the magnetic behavior of the **MnFe** compound.

4.2 Contribution of transition metal K-edge XMCD signal to the understanding of magnetic properties of matter.

In a general way, these results show that it is possible, by using an experimental original approach based on the use of model compounds such as PBAs, to establish quantitative relationships between the transition metal K-edge XMCD signals and local magnetic data. Furthermore, the versatility of PBAs, by making it possible to vary selected parameters independently, offers promising perspectives for a full quantitative interpretation of such signals in a near future. As a consequence, this also opens new perspectives towards quantitative investigation of local magnetic moments in systems which cannot be studied by transition metal $L_{2,3}$ edge XMCD. For instance, they are compounds sensitive to ultra-high vacuum containing volatile solvent molecules. For others, their surface is made of peculiar species due to surface effects or oxidation phenomena: transition metal $L_{2,3}$ edge XMCD probes the surface of materials, so that the main contribution to the signal can contain an important contribution from such peculiar surface species, preventing the investigation of the core species. They also are systems under demanding sample environment, for instance under high pressure or in operando conditions.

The series of studied compounds were chosen for their versatile chemical composition in analogous structures and their well-described magnetic properties by an orbital approach, suggesting comparable magnetic properties along the series. Nevertheless, the present XMCD study at the K-edges of the transition metal ions clearly reveals a peculiar local magnetic behavior of the Mn^{2+} ion in **MnFe**, that we propose to assign to a different orientation of the magnetic moment borne by the Mn^{2+} ion in **MnFe** with regard to that of the magnetic moments of all other A^{2+} ions along the series. This peculiar orientation of the Mn^{2+} magnetic moment in **MnFe** undoubtedly contributes to the peculiar macroscopic magnetic properties underlined in the section about the magnetic properties above. It has to be noted here that compounds containing $Mn[Fe(CN)_6]$ pairs attract interest from scientists in various field because they exhibit specific properties, among them photo-induced charge transfer[55] or magnetization reversal[56] properties. These properties are not completely understood and some of them could be related to the peculiar local magnetic behavior evidenced here.

At last, this suggests that transition metal K-edge XMCD could provide valuable information on the orientation of the local magnetic moments, including in compounds in powder form exhibiting a certain degree of disorder and containing water molecules, for which neutron diffraction measurements are so tricky. Work is in progress to better understand the origin of the $P_{h\nu}^A$ value and to establish a quantitative relationship between this value and the orientation of the local magnetic moments.

5. CONCLUSION

This study of the XMCD signal at the A K-edge in the two **AFe** and **ACr** PBAs series shows that the main 1s → 4p contribution to the A K-edge XMCD of PBAs does not depend on the magnetic neighbor of the A^{2+} ion, showing that the magnetic properties of the A^{2+} ion or of the A^{2+} sub-lattice are selectively probed. Furthermore its features can be related to the magnetic behavior of the probed A^{2+} ion or A^{2+} sub-lattice.

1) The shape of the signal can be related to the filling of the 3d orbitals. A derivative shape of the signal is associated with a same spin quantum number for all electrons in the 3d orbitals. A signal with one predominant lobe is obtained as soon as two electrons are paired, would it be due to a more than half-filled 3d shell in weak ligand field or to an electron pairing energy less than crystal field parameter.

2) The sign of the XMCD signal is related to the direction of the magnetic moment with respect to the applied magnetic field.

3) The XMCD absolute intensity is related in a quantitative way to the total spin quantum number S_A of the A^{2+} ion or of the A^{2+} sub-lattice.

4) The area under the XMCD peak is related in a quantitative way to the Curie constant C_A of the A^{2+} ion or of the A^{2+} sub-lattice.

This is, to our knowledge, the very first evidence that such quantitative information can be extracted from XMCD signals at the K-edges of the first transition metal series in molecular compounds. This is also the first time that the magnetic information contained in transition metal K-edge XMCD are clearly identified and related to a spectral feature of the XMCD signal.

It has to be noticed that such an analysis of the data has been made possible by a careful screening and mastering of all external parameters likely to affect the signal, as described in Ref. 40. Work is in progress i) to identify the parameters contained in $P_{h\nu}^A$ and better understand the origin of the peculiar behaviour of **MnFe** and ii) to analyze the K-edge XMCD signal at the B site of the coordination polymers.

This study at the A K-edge of PBA shows that PBA are model compounds particularly well suited to disentangle the information contained in XMCD signals at the TM K-edge and paves the way to the full understanding of these signals in

such molecular systems. Finally, we hope that such a study could be a starting point for new theoretical developments.

ASSOCIATED CONTENT

Supporting Information

The Supporting Information is available free of charge as a pdf file on the ACS Publications website. (S1 and S2 X-ray diffraction patterns, cell parameters and EDS analyses ; S3 and S5 Field Cooled (FC) and Zero Field Cooled (ZFC) magnetization curves ; S4 and S6 Temperature dependence of the inverse of the magnetic molar susceptibilities ; S7. XANES spectra at the A K-edge for the **AFe** and **ACr** series ; S8. A K-edge XAS spectra of **MnCr**, **MnFe**, **FeCr**, **CoCr**, **CoFe**, **NiCr**, **NiFe** and **CuFe** in the EXAFS range ; S9. XMCD signals belonging to the first group and to the second group for the **AFe** and the **ACr** series ; S10. Superimposition of the XMCD signals at the Fe K-edge of the compounds of the **AFe** series ; S11. Determination of the shape of the Fe K-edge XMCD signal of a Fe^{3+}(HS) ion from the linear combination of the XMCD signals of Berlin green and of **NiFe**.)

AUTHOR INFORMATION

Corresponding Author

*Anne.bleuzen@universite-paris-saclay.fr

Institut de Chimie Moléculaire et des Matériaux d'Orsay, CNRS, Université Paris-Saclay, 91405 Orsay, France

Author Contributions

The manuscript was written through contributions of all authors. / All authors have given approval to the final version of the manuscript. / All the authors contributed equally.
We are however sad to have to specify that our colleague, co-author and friend, François Baudelet, died on Jan. 28th 2022.

Funding Sources

Financial support was provided for the whole TM K-edge XMCD project and the PhD grant of A. N'Diaye by ANR MAgDiDi (ANR-17-CE29-0011), Paris-Saclay University and the CNRS. This research was carried also out with the support of the synchrotron SOLEIL.

ACKNOWLEDGMENT

The authors thank R. Saint-Martin and François Brisset (ICMMO) for technical support for XRD and EDS analyses, respectively, as well as E. Fonda, G. Landrot and A. Zitolo (SAMBA beamline, SOLEIL, France) for help during the XAS experiments. The authors also acknowledge SOLEIL for the provision of synchrotron radiation facility on the ODE beamline through proposals 20180264 and 20181406, and on the SAMBA beamline through proposals 20180264 and 20200652.

ABBREVIATIONS

LS, Low Spin; HS, High Spin; PBA, Prussian Blue Ananlog; XANES, X-ray Absorption Near-Edge Structure; EXAFS, Extended X-ray Absorption Fine Structure; MT, Transition Metal; ZFC, Zero Field Cooled; FC, Field Cooled; XMCD X-ray Magnetic Circular Dichroism.

REFERENCES

(1) van der Laan, G.; Figueroa A. I. X-ray magnetic circular dichroism—A versatile tool to study magnetism. *Coord. Chem. Rev.* 2014, *277–278*, 95.

(2) de Groot, F.M.F. X-ray absorption and dichroism of transition metals and their compounds. *J. Electron Spectroscopy and Related Phenomena* 1994, *61*, 529.

(3) Rogalev, A.; Wilhelm F. Magnetic circular dichroism in the hard X-ray range. *Phys. Metals Metallography* 2015, *116*, 1285.

(4) Thole, B. T.; Carra, P.; Sette F.; van der Laan G. X-ray circular dichroism as a probe of orbital magnetization. *Phys. Rev. Lett.* 1992, *68*, 1943.

(5) Carra, P.; Thole, B. T.; Altarelli M.; Wang X. X-ray circular dichroism and local magnetic fields. *Phys. Rev. Lett.* 1993, *70,* 694.

(6) Chen, C. T.; Idzerda, Y.U.; Lin, H.-J.; Smith, N. V.; Meigs, G.; Chaban, E.; Ho, G. H.; Pellegrin, E.; Sette, F. Experimental Confirmation of the X-Ray Magnetic Circular Dichroism Sum Rules for Iron and Cobalt. *Phys. Rev. Lett.* 1995, *75*, 152.

(7) Moroni, R.; Cartier dit Moulin, C.; Champion, G.; Arrio, M.-A.; Sainctavit, Ph.; Verdaguer, M.; Gatteschi, D. X-ray magnetic circular dichroism investigation of magnetic contributions from Mn(III) and Mn(IV) ions in Mn12-ac. *Phys. Rev. B* 2003, *68*, 064407.

(8) Schütz, G.; Wagner, W.; Wilhelm, W.; Kienle, P.; Zeller, R.; Frahm, R.; Materlik, G. Absorption of circularly polarized x rays in iron. *Phys. Rev. Lett.* 1987, *58*, 737.

(9) Torchio, R.; Mathon, O.; Pascarelli, S. XAS and XMCD spectroscopies to study matter at high pressure: Probing the correlation between structure and magnetism in the 3d metals. *Coord. Chem. Rev.* 2014, *277–278*, 80.

(10) Baudelet, F.; Pascarelli, S.; Mathon, O.; Itié, J.-P.; Polian, A.; d'Astuto, M.; Chervin, J.-C. X-ray absorption spectroscopy and x-ray magnetic circular dichroism simultaneous measurements under high pressure: the iron bcc–hcp transition case. *J. Phys. Condens. Matter* 2005, *17*, S957.

(11) Cafun, J.-D.; Lejeune, J.; Itié, J.-P.; Baudelet, F.; Bleuzen, A. XMCD at the Transition Metal K-Edges as a Probe of Small Pressure-Induced Structural Distortions in Prussian Blue Analogues. *J. Phys. Chem. C* 2013, *117*, 19645.

(12) Ishimatsu, N.; Shichijo, T.; Matsushima, Y.; Maruyama, H.; Matsuura, Y.; Tsumuraya, T.; Shishidou, T.; Oguchi, T.; Kawamura, N.; Mizumaki, M.; Matsuoka, T.; Takemura, K. Hydrogen-induced modification of the electronic structure and magnetic states in Fe, Co, and Ni monohydrides. *Phys. Rev. B* 2012, *86*, 104430.

(13) Torchio, R.; Kvashnin, Y. O.; Pascarelli, S.; Mathon, O.; Marini, C.; Genovese, L.; Bruno, P.; Garbarino, G.; Dewaele, A.; Occelli, F.; Loubeyre, P. X-Ray Magnetic Circular Dichroism Measurements in Ni up to 200 GPa: Resistant Ferromagnetism. *Phys. Rev. Lett* 2011, *107*, 237202.

(14) Torchio, R.; Monza, A.; Baudelet, F.; Pascarelli, S.; Mathon, O.; Pugh, E.; Antonangeli, D.; Itié, J.-P. Pressure-induced collapse of ferromagnetism in cobalt up to 120 GPa as seen via x-ray magnetic circular dichroism. *Phys. Rev. B* 2011, *84*, 060403(R).

(15) Igarashi, J. I.; Hirai, K. Orbital moment and magnetic circular dichroism at the *K* edge in ferromagnetic cobalt. *Phys. Rev. B* 1996, *53*, 6442.

(16) Bouldi, N.; Vollmers, N. J.; Delpy-Laplanche, C. G.; Joly, Y.; Juhin, A.; Sainctavit, Ph.; Brouder, Ch.; Calandra, M.; Paulatto, L.; Mauri, F.; Gerstmann, U. X-ray magnetic and natural circular dichroism from first principles: Calculation of K- and L1-edge spectra. *Phys. Rev. B* 2017, *96,* 085123.

(17) Ebert, H. Influence of the orbital polarization on the magnetic X-ray dichroism of transition metals. *Solid State Commun.* 1996, *100*, 677.

(18) Stähler, S.; Schütz G.; Ebert, H. Magnetic *K*-edge absorption in 3*d* elements and its relation to local magnetic structure. *Phys. Rev. B* 1993, *47*, 818.

(19) Gotsis, H. J.; Strange, P. A first-principles theory of X-ray Faraday effects. *J. Phys. Condens. Matter* 1994, *6*, 1409.

(20) Guo, G. Y. What does the K-edge x-ray magnetic circular dichroism spectrum tell us? *J. Phys. Condens. Matter* 1996, *8*, L747.

(21) Brouder, Ch.; Hikam, M. Multiple-scattering theory of magnetic x-ray circular dichroism. *Phys. Rev. B* 1991, *43*, 3809.

(22) Brouder, Ch.; Alouani, M.; Bennemann, K. H. Multiple-scattering theory of x-ray magnetic circular dichroism: Implementation and results for the iron *K* edge. *Phys. Rev. B* 1996, *54*, 7334.

(23) Natoli, C. R.; Benfatto, M.; Doniach, S. Use of general potentials in multiple-scattering theory. *Phys. Rev. A* 1986, *34*, 4682.

(24) Joly, Y.; Bunau, O.; Lorenzo, J. E.; Galéra, R. M.; Grenier, S.; Thompson, B. Self-consistency, spin-orbit and other advances in the FDMNES code to simulate XANES and RXD experiments. *J. Phys. Conf. Ser.* 2009, *190*, 012007.

(25) Arrio, M.-A.; Sainctavit, Ph.; Cartier dit Moulin, Ch.; Brouder, Ch.; de Groot, F.M.F.; Mallah T.; Verdaguer, M. *Physica B*. Soft X-ray magnetic circular dichroism in molecular based magnet. 1995, *208-209*, 775.

(26) Arrio, M.-A.; Sainctavit, Ph.; Cartier dit Moulin, Ch.; Brouder, Ch.; de Groot, F. M. F.; Mallah, T.; Verdaguer, M. Measurement of Magnetic Moment at the Atomic Scale in a High TC Molecular Based Magnet. *J. Phys. Chem.* 1996, *100*, 4679.

(27) Arrio, M.-A.; Long, J.; Cartier dit Moulin, C.; Bachschmidt, A.; Marvaud, V.; Rogalev, A.; Mathonière, C.; Wilhelm, F.; Sainctavit, Ph. Photoinduced Magnetization on Mo Ion in Copper Octacyanomolybdate: An X-ray Magnetic Circular Dichroism Investigation. *J. Phys. Chem. C* 2010, *114*, 593.

(28) Jafri, S. F.; Koumousi, E. S.; Arrio, M.-A.; Juhin, A.; Mitcov, D.; Rouzières, M.; Dechambenoit, P.; Li, D.; Otero, E.; Wilhelm, F.; Rogalev, A.; Joly, L.; Kappler, J.-P.; Cartier dit Moulin, C.; Mathonière, C.; Clérac, R.; Sainctavit, Ph. Atomic Scale Evidence of the Switching Mechanism in a Photomagnetic CoFe Dinuclear Prussian Blue Analogue. *J. Am. Chem. Soc.* 2019, *141*, 3470.

(29) Coronado, E.; Carmen Gimenez-Lopez, M.; Korzeniak, T.; Levchenko, G.; Romero, F. M.; Segura, A.; Garcia Baonza, V.; Cezar, J. C.; de Groot, F. M. F.; Milner, A.; Paz-Pasternak, M. Pressure-Induced Magnetic Switching and Linkage Isomerism in K0.4Fe4[Cr(CN)6]2.8·16H2O: X-ray Absorption and Magnetic Circular Dichroism Studies. *J. Am. Chem. Soc.* 2008, *130*, 15519.

(30) Prado, Y.; Arrio, M.-A.; Volatron, F.; Otero, E.; Cartier dit Moulin, C.; Sainctavit, Ph.; Catala, L.; Mallah, T. Magnetic Anisotropy of Cyanide-Bridged Core and Core–Shell Coordination Nanoparticles Probed by X-ray Magnetic Circular Dichroism. *Chem. Eur. J.* 2013, *19*, 6685.

(31) Jafri, S. F.; Arrio, M.-A.; Bordage, A.; Moulin, R.; Juhin, A.; Cartier dit Moulin, C.; Otero, E.; Ohresser, P.; Bleuzen, A.; Sainctavit, Ph. Weak ferromagnetic interaction at the surface of the ferrimagnetic $Rb_2Co_4[Fe(CN)_6]_{3.3}\cdot 11H_2O$ photo-excited state. *Inorg. Chem.* 2018, *57*, 7610.

(32) Dujardin, E.; Ferlay, S.; Phan, X.; Desplanches, C.; Cartier dit Moulin, C.; Sainctavit, Ph.; Baudelet, F.; Dartyge, E.; Veillet, P.; Verdaguer, P. Synthesis and Magnetization of New Room-Temperature Molecule-Based Magnets: Effect of Stoichiometry on Local Magnetic Structure by X-ray Magnetic Circular Dichroism. *J. Am. Chem. Soc.* 1998, *120*, 11347.

(33) Keggin, J. F.; Miles, F. D. Structures and Formulæ of the Prussian Blues and Related Compounds. *Nature* 1936, *137*, 577.

(34) Lüdi, A.; Güdel, H. U. Structural chemistry of polynuclear transition metal cyanides. *Structure and Bonding;* Springer-Verlag Berlin 1973*, 14,* 1.

(35) Buser, H. J; Ludi, A; Petter, W.; Schwarzenbach, D. The crystal structure of Prussian Blue: $Fe_4[Fe(CN)_6]_3\cdot xH_2O$. *Inorg. Chem.* 1977*, 16,* 2704.

(36) Simonov, A.; De Baerdemaeker, T.; Boström, H. L. B.; Ríos Gómez, M. L.; Gray, H. J.; Chernyshov, D.; Bosak, A.; Bürgi, H.-B.; Goodwin, A. L. Hidden diversity of vacancy networks in Prussian blue analogues. *Nature* 2020 , *578* , 256.

(37) Briois, V.; Fonda, E.; Belin, S.; Barthe, L.; La Fontaine, C.; Langlois, F.; Ribens, M.; Villain, F. SAMBA: The 4–40 keV X-ray absorption spectroscopy beamline at SOLEIL. *UVX 2010 EDP Sciences* 2011, 41.

(38) Ravel, B.; Newville, M. *ATHENA*, *ARTEMIS*, *HEPHAESTUS*: data analysis for X-ray absorption spectroscopy using *IFEFFIT*. *J. Synchrotron Rad.* 2005, *12*, 537.

(39) Baudelet, F.; Kong, Q.; Nataf, L.; Cafun, J.-D.; Congedutti, A.; Monza, A.; Chagnot, S.; Itié, J.-P. ODE: a new beam line for high-pressure XAS and XMCD studies at SOLEIL. *High Pressure Research* 2011, *31*, 136.

(40) N'Diaye, A.; Bordage, A.; Nataf, L.; Baudelet, F.; Bleuzen, A. A cookbook for the investigation of coordination polymers by transition metal K-edge XMCD. *J. Synchrotron Rad.* 2021, *28*, 1127.

(41) Hallmeier, K. H.; Sauter, S.; Szargan, R. XANES and EXAFS investigations of bonding and structure of Ni and Co derivatives from Prussian Blue coordination compounds. *J. Inorg. Chem. Comm.* 2001, *4*, 153.

(42) Kosugi, N.; Yokohama, T.; Asakura, K.; Kuroda, H. Polarized Cu K-edge XANES of square planar $CuCl_4^{2-}$ ion. Experimental and theoretical evidence for shake-down phenomena. *Chem. Phys.* 1984, *91*, 249.

(43) Smith, T. A.; Penner-Hahn, J. E.; Herding, M. A. ; Doniach, S.; Hodgson, K. O. Polarized X-ray Absorption Edge Spectroscopy of Single-Crystal Copper(II) Complexes. *J. Am. Chem. Soc.* 1985, *107*, 5945.

(44) Shadle, S. E.; Penner-Hahn, J. E.; Schugar, H. J.; Hedman, B.; Hodgson, K. O.; Solomon, E. I. X-ray absorption spectroscopic studies of the blue copper site: metal and ligand K-edge studies to probe the origin of the EPR hyperfine splitting in plastocyanin. *J. Am. Chem. Soc.* 1993, *115*, 767.

(45) Verdaguer, M.; Mallah, T.; Hélary, C.; L'Hermite, F.; Sainctavit, Ph.; Arrio, M.A.; Babel, D.; Baudelet, F.; Dartyge, E.; Fontaine, A. K edge X-ray magnetic circular dichroism in molecule-based magnets. *Physica B* 1995, *208-209*, 765.

(46) Lahiri, D.; Choi, Y.; Yusuf, S.M.; Kumar, A.; Ramanan, N.; Chattopadhyay, S.; Haskel, D.; Sharma, S. M. Understanding temperature and magnetic-field actuated magnetization polarity reversal in the Prussian blue analogue $Cu_{0.73}Mn_{0.77}[Fe(CN)_6].zH_2O$, using XMCD. *Mater. Res. Express* 2016, *3*, 036101.

(47) Herrera, J. M.; Bachschmidt, A.; Villain, F.; Bleuzen, A.; Marvaud, V.; Wernsdorfer, W.; Verdaguer, M. Mixed valency and magnetism in cyanometallates and Prussian blue analogues. *Phil. Trans. R. Soc. A* 2008, *366*, 127.

(48) Mallah, T.; Ferlay, S.; Auberger, C.; Hélary, C.; L'Hermite, F.; Ouahès, R.; Vaissemann, J.; Verdaguer, M.; Veillet, P. Hexacyanometalates: Molecular Precursors for High-Spin Molecules and High-TC Molecule-Based Magnets. *Mol. Cryst. Liq. Cryst.* 1995, *273*, 141.

(49) Escax, V.; Cartier dit Moulin, C.; Villain, F.; Champion, G.; Itié, J.-P.; Münsch, P.; Verdaguer, M.; Bleuzen, A. Photo-induced Ferrimagnetic Systems in Prussian Blue Analogues $X^I_xCo_4[Fe(CN)_6]_y$ (X^I = alkali cation). *C. R. Chimie* 2003, *6*, 1165.

(50) Champion, G.; Escax, V.; Cartier dit Moulin, C.; Bleuzen, A.; Villain, F.; Baudelet, F.; Dartyge, E.; Verdaguer, M. Photo-Induced Ferrimagnetic systems in Prussian Blue Analogs $C^I_xCo_4[Fe(CN)_6]_y$ (C^I=alkali cation). 4. Characterization of the ferrimagnetism of the photo-induced Metastable state in $Rb_{1.8}Co_4[Fe(CN)_6]_{3.3}\bullet 13H_2O$ by K Edges X-Ray Magnetic Circular Dichroism. *J. Am. Chem. Soc.* 2001, *123*, 12544.

(51) Bordage, A.; Nataf, L.; Baudelet, F.; Bleuzen, A. Investigation of Prussian Blue Analogs by XMCD at the K-edge of transition metals. *J. Phys.: Conference Series* 2016, *712*, 012109.

(52) Kumar, A.; Yusuf, S. M. Structural and magnetic properties of $Fe[Fe(CN)_6]\cdot 4H_2O$. *Phys. Rev. B* 2005, *71*, 054414.

(53) Pizzini, S; Bonfim, M.; Baudelet, F.; Tolentino, H.; San Miguel, A.; Mackay, K.; Malgrange, C.; Hagelsein, M.; Fontaine, A. Quarter-Wave Plates and X-ray Magnetic Circular Dichroism on ID24 at the ESRF. *J. Synchrotron Rad.* 1998, *5*, 1298

(54) Escax, V.; Bleuzen, A.; Cartier dit Moulin, C.; Villain, F.; Goujon, A.; Varret, F.; Verdaguer, M. Photo-Induced Ferrimagnetic systems in Prussian Blue Analogs $C^I_xCo_4[Fe(CN)_6]_y$ (C^I=alkali cation). 3. Why and How the Efficiency of the Photoinduced Process depends on a Compromise between Co-Fe Diamagnetic Pairs and $[Fe(CN)_6]$ Vacancies. *J. Am. Chem. Soc.* 2001, *123*, 12536.

(55) Ohkoshi, S.-I.; Tokoro, H.; Hashimoto, K. Temperature- and photo- induced phase transition in rubidium manganese hexacyanoferrate. *Coord. Chem. Rev.* 2005, *249*, 1830.

(56) Kumar, A. ; Yusuf, S. M. ; Keller, L. ; Yakhmi, J.V. Microscopic Understanding of Negative Magnetization in Cu, Mn, and Fe Based Prussian Blue Analogues. *Phys. Rev. Lett.* 2008, *101*, 207206.

TOC Synopsis

A better understanding of transition metal K-edge X-ray Magnetic Circular Dichroism is obtained thanks to an experimental approach based on the versatile chemical composition of Prussian Blue Analogs. Qualitative and quantitative parameters of the main signal are related to the magnetic behavior of the absorbing atom: shape and sign to the filling of the 3d orbitals and to the direction of the magnetic moment; intensity and area-under-peak to the total spin and to the Curie constant.

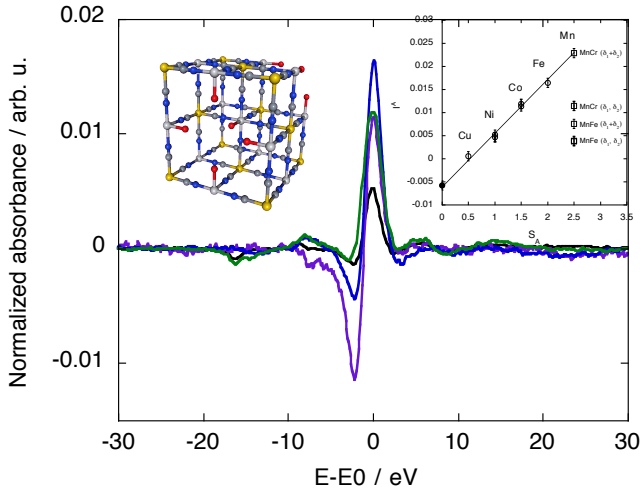

Insert Table of Contents artwork here